Thomas Sattel[1]
Mechatronics Group,
Department of Mechanical Engineering,
Ilmenau University of Technology,
Max-Planck-Ring 12,
Building F,
98684 Ilmenau, Germany
e-mail: thomas.sattel@tu-ilmenau.de

Peter Hagedorn
Fellow ASME

Joachim Schmidt

Dynamics and Vibrations Group,
Department of Mechanical Engineering,
Darmstadt University of Technology,
64289 Darmstadt, Germany

The Contact Problem in Ultrasonic Traveling-Wave Motors

In this paper the contact mechanism between stator and rotor will be considered in detail, which plays a key role in ultrasonic motors. A planar contact model for the stator-rotor interaction in traveling-wave type ultrasonic motors is derived, including rotor flexibility and differenciating between stick and slip regions in the contact zones. The model analysis shows that depending on the motor's operating conditions, complicated contact behavior may occur with several stick-slip subzones in each contact zone. The typical nonlinear resonance observed in ultrasonic motors can be explained with the present analysis. Both the stiffness of the contact layer and of the rotor may drastically influence the speed-torque characteristics. The results will contribute to a better understanding of the contact mechanics in ultrasonic motors. [DOI: 10.1115/1.4000380]

Keywords: ultrasonic motor, piezoelectric motor, contact, traveling-wave, stick, slip, speed-torque characteristic

1 Background

The mechanics of ultrasonic traveling-wave motors (USMs) contains a number of problems, which have not been modeled yet in detail. The contact problem between stator and rotor is probably the most important one. Though several models have been proposed in the past, the contact problem is usually oversimplified. Experimental investigations show that rotor flexibility strongly influences torque-speed characteristics. Additionally, assuming a pure slip law for the tangential contact overestimates the frictional losses in the motor. A comprehensive survey of the state of the art of stator-rotor contact in USMs is given by Wallaschek [1]. Zharii and Ulitko [2], and Le Moal and Minotti [3] applied the half-space method. The former paper assumes a rigid rotor, while the latter assumes the stator as a rigid intender with a sinusoidal profile and ignores the inertias of the rotor and the contact layer. Cao and Wallaschek [4] modeled the rotor as a rigid body, and the stator motion was prescribed. For the normal contact a visco-elastic material law was chosen, whereas the contact layer was modeled as rigid in tangential direction. Within one contact zone they found up to three driving and braking contact subzones. Schmidt et al. [5] chose a similar model as proposed in Ref. [4]. It was shown that the feedback of the rotor on the stator motion is negligible in the vicinity of resonance. In Ref. [6] a complete motor model based on design parameters was proposed, where the rotor was modeled as a rigid body with one rotational and one axial degree of freedom. A pure slip law was assumed for the contact. Hagedorn et al. [7] extended this motor model by incorporating rotor flexibility. It turns out that the measured torque-speed characteristics cannot be matched when rotor flexibility is ignored, while good results are obtained including the flexibility of the rotor in the model.

The aforementioned models have led to a deeper and better understanding of USMs. Measured torque-speed characteristics are, for example, reproduced well by these simplified contact models if only a few of the model parameters are adjusted accordingly. A more detailed modeling is achieved by using a contact model with compliance both in normal and tangential direction, distinguishing between stick and slip-contact states and by incorporating rotor flexibility in the contact model. If, for example, particular torque-speed characteristics are desired, such models shall give guidelines how to choose the proper motor parameters. Also, in order to improve the motor efficiency a detailed description of the contact behavior between stator and rotor would be helpful, since measurements of the contact state between stator and rotor are difficult to carry out.

A typical plate-type USM with the operational eigenmode of the stator is shown in Fig. 1. A detailed description of the working principle of this motor is found in Ref. [8] or Ref. [9], for example. The stator is clamped at the inner radius and free at the outer radius, $r_i = 10$ mm and $r_a = 30$ mm. By electrical excitation of a piezoceramic ring, which is bonded to the lower surface of the stator, a bending-wave of the shape illustrated in Fig. 1 is excited in the stator, traveling in the circumferential direction. The traveling bending-wave is obtained by appropriate excitation of two degenerated bending modes excited in resonance with a circular frequency Ω and a temporal phase shift of 90 deg. The excitation frequency of USMs is above 20 kHz, and the vibration amplitudes in the stator usually are in the micron range. The stator behaves as a plate-type structure. Thus, the traveling bending-wave causes points on the stator surface to run through elliptic trajectories. With the rotor pressed against the stator, frictional forces in the contact zones produce the torque that drives the rotor. It is the objective of this paper to investigate the steady-state motor operation of ultrasonic traveling-wave motors under simplifying assumptions but including a contact model with a visco-elastic contact layer both for normal and tangential contact, stick and slip tangential contact, and rotor flexibility.

2 Modeling

The contact between stator and rotor takes place in a small strip $r \in [r_a - s, r_a]$ of width $s \ll r_a$, in the vicinity of the outer radius r_a. Here s is the width of the contact layer depicted in Fig. 1. To simplify basic understanding and computation, the radial displacements and contact forces are ignored, and the lateral and tangential displacements and contact forces are assumed to be constant for $r \in [r_a - s, r_a]$. Hence, stator and rotor may be described by a planar model, as for example by straight Bernoulli–Euler beams with periodic boundary conditions, see Fig. 2. But note that for an overall motor optimization, it is important to take the radial contact pressure distribution into account, especially with respect to wear effects.

The proposed planar contact model, as shown in Fig. 2, is based on the kinematics of USMs comparable to Shinsei USR motors.

[1]Corresponding author.

Contributed by the Applied Mechanics of ASME for publication in the JOURNAL OF APPLIED MECHANICS. Manuscript received January 17, 2004; final manuscript received July 24, 2009; published online February 23, 2010. Editor: Robert M. McMeeking.

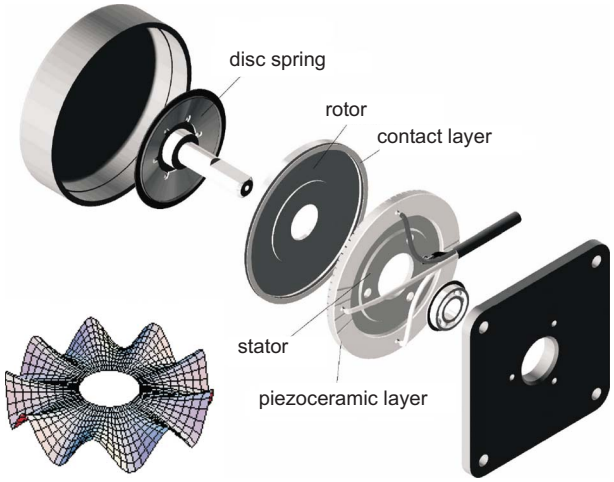

Fig. 1 Shinsei USR60 ultrasonic traveling-wave motor

Such motors have n_w wave-trains along the circumference. Thus, at steady-state motor operation, n_w, contact zones at the outer radius occur in the circumferential direction. Since the system is periodic (period λ), it is sufficient to model only one contact zone. Both stator and rotor rest on elastic foundations with stiffnesses k_s and k_r, respectively, and are modeled using the Bernoulli–Euler beam theory. The stator and rotor have bending stiffnesses E_sI_s and E_rI_r, respectively. The cross sections are A_s and A_r, the beam heights are h_s and h_r, and the mass densities are denoted as ρ_s and ρ_r. The contact layer is described by the parameters E_c, ϑ_c, G_c, and η_c, which represent Young's modulus, the viscous-damping coefficient, the shear modulus, and the viscous shear damping coefficient, respectively. The effect of the electrical excitation of the piezoceramic sections on the deformation of the stator substrate can be substituted by localized external bending moments $\hat{M}$. The axial pressure p forces the rotor and stator together. The contact layer in Fig. 4 is modeled as a point-visco-elastic foundation in normal and tangential directions.

2.1 Kinematics. In the planar contact model, shown in Figs. 2 and 3, three reference frames are taken: a laboratory fixed, (O,x,z), a rotor fixed, $(\bar{O},\bar{x},\bar{z})$, and a traveling-wave fixed reference frame $(\tilde{O},\tilde{x},\tilde{z})$, as chosen also by Cao and Wallaschek [4].

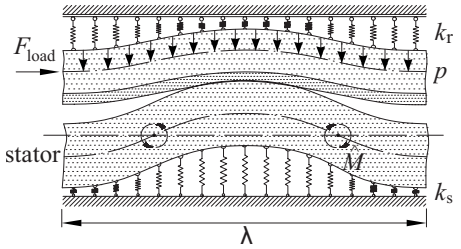

Fig. 2 Planar stator-rotor contact model

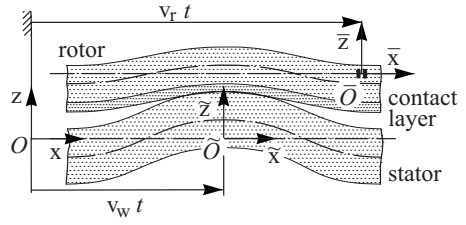

Fig. 3 Deformed configuration and reference frames

The origins O and $\bar{O}$ are located on the neutral axis of the stator and the rotor, respectively, in the reference configuration, i.e., the configuration without external loads. Taking x as the axial coordinate of the straight beam model (corresponding to $x=r_a\varphi$) with the outer circumferential length $L=2\pi r_a$, the displacements of stator, rotor, and contact layer, $\mathbf{u}_s$, $\mathbf{u}_r$, and $\mathbf{u}_c$, respectively, are given by

$$\mathbf{u}_s(x,z,t) = -zw_s'(x,t)\mathbf{e}_x + w_s(x,t)\mathbf{e}_z \tag{1}$$

$$\bar{\mathbf{u}}_r(\bar{x},\bar{z},t) = -\bar{z}\bar{w}_r'(\bar{x},t)\mathbf{e}_x + \bar{w}_r(\bar{x},t)\mathbf{e}_z \tag{2}$$

$$\bar{\mathbf{u}}_c(\bar{x},\bar{z},t) = \bar{\mathbf{u}}_r(\bar{x},\bar{z},t) + [\bar{u}_c(\bar{x},t)\mathbf{e}_x + \bar{w}_c(\bar{x},t)\mathbf{e}_z] \tag{3}$$

where the prime denotes the derivative with respect to the coordinates x and $\bar{x}$, respectively. The excitation and superposition of two orthogonal bending modes in the stator with a temporal phase shift of 90 deg results in

$$w_s(x,t) = \hat{w}\cos kx\cos\Omega t \pm \hat{w}\sin kx\sin\Omega t = \hat{w}\cos(kx-\Omega t),$$

$$k = \frac{2\pi}{\lambda}, \quad \lambda = \frac{L}{n_w} \tag{4}$$

with k being the wave number, n_w being the number of nodal diameters, and λ being the wavelength. Substituting Eq. (4) into Eq. (1) results in elliptic trajectories of stator surface points. According to Eq. (4) the traveling-wave speed of the bending-wave in the stator and the wave fixed reference frame $(\tilde{O},\tilde{x},\tilde{z})$ is given by

$$v_w = \frac{\Omega}{k} \tag{5}$$

The reference frame $(\bar{O},\bar{x},\bar{z})$ is defined to move with positive rotor speed, v_r, in the positive $\mathbf{e}_x$-direction. Note that the rotor speed, v_r, has an opposite sign to the traveling-wave speed, v_w, due to the special kinematics of the bending deformation in Bernoulli–Euler beam models. The coordinate transformations between the coordinates of the different reference frames are

$$\bar{x} = x - v_r t, \quad \bar{z} = z - \frac{h_s}{2} - h_c - \frac{h_r}{2} \tag{6}$$

$$\tilde{x} = x - v_w t, \quad \tilde{z} = z \tag{7}$$

$$\tilde{x} = \bar{x} + v_d t, \quad \tilde{z} = \bar{z} + \frac{h_s}{2} + h_c + \frac{h_r}{2} \quad \text{with} \quad v_d := v_r - v_w = v_r - \frac{\Omega}{k} \tag{8}$$

The displacements of stator, rotor and contact layer will be expressed in coordinates of the traveling-wave fixed reference frame. In this reference frame the harmonic traveling-wave degenerates into a standing wave. For the stator displacement one gets

$$\tilde{w}_s(\tilde{x},t) := w_s(\tilde{x}-v_w t,t) \tag{9}$$

The time derivative, $\dot{(\cdot)}$, with respect to the laboratory fixed reference frame (O,x,z) results in

$$\dot{\tilde{w}}_s(\tilde{x},t) = \mathring{\tilde{w}}_s(\tilde{x},t) - v_w\tilde{w}_s'(\tilde{x},t) \tag{10}$$

where $\mathring{(\cdot)}$ represents the time derivative with respect to the traveling-wave fixed reference frame. In the vicinity of the motor's resonance and in the steady-state motor operation $\mathring{(\cdot)}=0$ is assumed. For the time derivatives of the rotor and contact layer displacements similar relations as Eq. (10) hold. Note that for the motor operating near resonance peak, higher order harmonics of the excitation frequency are neglected.

The displacement functions of all surface points of stator and contact layer are therefore defined as

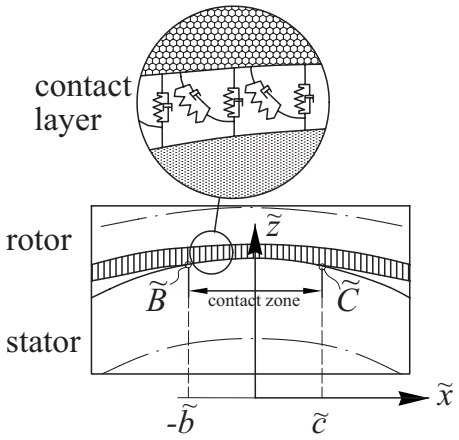

Fig. 4 Contact layer model

$$\hat{\mathbf{u}}_s(x,t) := \mathbf{u}_s\left(x, \frac{h_s}{2}, t\right), \quad \hat{\bar{\mathbf{u}}}_c(\bar{x},t) := \bar{\mathbf{u}}_c(\bar{x},\bar{h},t) \quad \text{with} \quad \bar{h} = -\frac{h_r}{2} - h_c \tag{11}$$

where it should be clear that throughout the modeling a hat symbol $\hat{(\cdot)}$ indicates a field variable on a surface. After carrying out a coordinate transformation according to Eqs. (7) and (8), the displacement of stator and contact layer surface points $\hat{\tilde{\mathbf{u}}}_s(\tilde{x},t)$ and $\hat{\tilde{\mathbf{u}}}_c(\tilde{x},t)$ are obtained. The velocities of surface points under steady-state conditions are derived according to Eq. (10)

$$\hat{\tilde{\mathbf{v}}}_s(\tilde{x}) := \dot{\hat{\tilde{\mathbf{u}}}}_s(\tilde{x}) = -v_w \tilde{w}_s'(\tilde{x})\mathbf{e}_z + \frac{h_s}{2} v_w \tilde{w}_s''(\tilde{x})\mathbf{e}_x \tag{12}$$

$$\hat{\tilde{\mathbf{v}}}_c(\tilde{x}) := \dot{\hat{\tilde{\mathbf{u}}}}_c(\tilde{x}) = [v_r + v_d \bar{h}\tilde{w}_r''(\tilde{x}) + v_d \tilde{u}_c'(\tilde{x})]\mathbf{e}_x + v_d[\tilde{w}_r'(\tilde{x}) + \tilde{w}_c'(\tilde{x})]\mathbf{e}_z \tag{13}$$

A geometrical contact formulation with a nonpenetration condition is chosen for considering normal contact, see Ref. [10]. This implies only a small penetration of the midlines of the rough surfaces. Such an assumption is justified by the facts that, on one hand, the contacting surfaces are surface finished to reduce the average surface roughness to values smaller than the vibration amplitudes in the stator. On the other hand, the contact pressure between stator and rotor is usually in the range of only several $\mathrm{N/mm^2}$, which can be regarded as a low-level contact pressure, see, e.g., Refs. [11–13].

When using geometric linear kinematics, the coordinates of two contacting surface points $(\tilde{x}_P, \tilde{x}_Q)$ of stator and contact layer, nearly coincide, $\tilde{x}_P \approx \tilde{x}_Q \approx \tilde{x}$. Therefore, the relations $\hat{\tilde{\mathbf{u}}}_s(\tilde{x})\mathbf{e}_z = \hat{\tilde{\mathbf{u}}}_c(\tilde{x})\mathbf{e}_z$, $\hat{\tilde{\mathbf{v}}}_s(\tilde{x})\mathbf{e}_z = \hat{\tilde{\mathbf{v}}}_c(\tilde{x})\mathbf{e}_z$ hold for the normal contact in the $\mathbf{e}_z$-direction, yielding

$$\tilde{w}_s - \tilde{w}_r - \tilde{w}_c = 0 \tag{14}$$

$$v_w \tilde{w}_s' + v_d(\tilde{w}_r' + \tilde{w}_c') = 0 \tag{15}$$

The relative velocity for the tangential contact can be defined as $v_{\mathrm{rel}}(\tilde{x}) := [\hat{\tilde{\mathbf{v}}}_s(\tilde{x}) - \hat{\tilde{\mathbf{v}}}_r(\tilde{x})] \cdot \mathbf{e}_x$, leading to

$$\tilde{v}_{\mathrm{rel}} = \frac{h_s}{2} v_w \tilde{w}_s'' - (v_r + v_d \bar{h}\tilde{w}_r'' + v_d \tilde{u}_c') \tag{16}$$

A visco-elastic contact layer exhibits a spatial phase shift between the wave-crest and $\tilde{z}$-axis. Therefore, the contact boundaries $(\tilde{B}, \tilde{C})$ in Fig. 4 have different coordinates. The bending-wave is assumed to travel in the positive $\tilde{x}$-direction according to Eq. (4), and thus surface points of stator and contact layer to the right of $\tilde{x}=\tilde{c}$ approach each other. Conversely, points to the left of $\tilde{x}=-\tilde{b}$ separate from each other. The *contact length* is $\tilde{b}+\tilde{c}$. Therefore, locations $\tilde{x}=\tilde{c}$ and $\tilde{x}=-\tilde{b}$ represent the *beginning* (point $\tilde{C}$) and *end* (point $\tilde{B}$) of the contact zone, respectively. The periodic boundary conditions are formulated at $\tilde{x}=-\lambda/2$ and $\tilde{x}=\lambda/2$.

2.2 Dynamics

2.2.1 Hamilton's Principle. The equations of motion of the contact model are derived from Hamilton's principle

$$\int_{t_1}^{t_2} (\delta L + \delta W)dt = 0 \quad \text{with} \quad L := T - U \tag{17}$$

The Lagrange function, L, consists of the kinetic and potential energy of stator, rotor, and contact layer

$$L = (T_s + T_r + T_c) - (U_s + U_r) \tag{18}$$

Since for the contact layer height $h_c \ll h_s$ and $h_c \ll h_r$ holds, one can assume in a first approximation that the kinetic energy term of the contact layer is much smaller than the contributions of the other kinetic energy terms. Thus, we set $T_c=0$. No potential energy term for the contact layer is defined since we will use a visco-elastic foundation model for this layer, using the virtual work of its inner forces and not the internal energy.

The virtual work, δW, is broken up into several terms representing contributions due to forces acting on the stator, δW_s, the rotor, δW_r, and the contact layer, δW_c

$$\delta W = (\delta W_{s_m} + \delta W_{s_d} + \delta W_{s_c}) + \delta W_{r_p} + (\delta W_{c_i} + \delta W_{c_c}) \tag{19}$$

The various energy and work expressions are given below.

2.3 Stator Energy and Work Terms. The terms of kinetic and potential energy of a Bernoulli–Euler beam are

$$T_s = \tfrac{1}{2}\int_0^{n_w\lambda} \rho_s A_s \dot{w}_s^2 dx, \quad U_s = \tfrac{1}{2}\int_0^{n_w\lambda} \left[E_s I_s w_s''^2 + \tfrac{1}{2}k_s w_s^2\right]dx \tag{20}$$

The stator rests on an elastic foundation with stiffness k_s. Note that the integration is carried out over the length $L=n_w\lambda$ of the beam model. The virtual work due to the bending moment excitation may be written as

$$\delta W_{s_m} = \int_0^{n_w\lambda_s} -M(x,t)\,\delta w_s'' dx \tag{21}$$

The bending moment excitation, $M(x,t)$, is chosen to act symmetric with respect to the $\tilde{z}$-axis of the traveling-wave fixed reference frame (see Figs. 3 and 4). Thus, the $\tilde{z}$-axis intersects with the wave-crest of the traveling bending-wave for an elastic contact layer. The bending moment distribution shall travel with the wave speed v_w from the left to the right. In coordinates of the traveling-wave fixed reference frame this leads to

$$\tilde{M}(\tilde{x}) = \hat{M}\sum_{j=0}^{n_w} \left((-1)^j 2\left[\mathrm{h}\left(\tilde{x} + \frac{(2j+1)\lambda}{4}\right) - \mathrm{h}\left(\tilde{x} - \frac{(2j+1)\lambda}{4}\right)\right] - 1\right) \tag{22}$$

where h is the step function. The practical realization of such a traveling bending-wave is not important for what follows. The contact force $\mathbf{F}_c$ with the normal and tangential contact force components acting on the stator produce the virtual work

$$\delta W_{s_c} = \int_0^{n_w\lambda} \mathbf{F}_c \delta\hat{\tilde{\mathbf{u}}}_s dx \quad \text{with} \quad \mathbf{F}_c(x,t) := -F_T(x,t)\mathbf{e}_x - F_N(x,t)\mathbf{e}_z$$

$$[F_N] = [F_T] = [\mathrm{N/m}] \tag{23}$$

Inner damping mechanisms within the stator substrate and the piezoceramic material are described by a visco-elastic damping law

$$\delta W_{s_d} = \int_0^{n_w\lambda} \eta_s E_s I_s \dot{w}_s'' \delta w_s'' dx \tag{24}$$

with loss factor η_s.

2.4 Rotor Energy Terms. As it was done for the stator, the terms of the rotor kinetic and potential energy may be formulated as

$$T_r = \tfrac{1}{2}\int_0^{n_w\lambda} \rho_r A_r [v_r^2 + \dot{\bar{w}}_r^2] d\bar{x}, \quad U_r = \tfrac{1}{2}\int_0^{n_w\lambda} [E_r I_r (\bar{w}_r'')^2 + k_r \bar{w}_r^2] d\bar{x} \tag{25}$$

where k_r is the stiffness of the rotor's elastic foundation. The difference here is that the spatial integration is carried out with respect to the coordinates of the reference frame $(\bar{O}, \bar{x}, \bar{z})$, fixed to the rotor rigid body motion in the $\mathbf{e}_x$-direction. The axial pressure, pressing the rotor against the stator, yields the virtual work term

$$\delta W_{rp} = -\int_0^{n_w\lambda} p(\bar{x})\, \delta \bar{w}_r d\bar{x}, \quad p(\bar{x}) = \frac{F_{\mathrm{axial}}}{n_w \lambda} \tag{26}$$

2.4.1 Contact Layer Work. In USMs a special contact material between stator and rotor is often used to improve such features as the maximum torque or wear properties, for example. Polymer materials are mostly used for this purpose. In Ref. [14], p. 288, several of these contact layer materials are described. More detailed investigations concerning contact layer materials have been conducted by Rehbein and Wallaschek [15]. For the polymer materials at harmonic loading cycles, a simplified form of a Kelvin–Voigt material model is used. In the point-visco-elastic foundation model depicted in Fig. 4 neighboring particles are decoupled, i.e., they have no influence to each other. Indeed, from a modeling point of view and applying linear theory of visco-elasticity, it turns out that the coupling between neighboring particles is negligible for thin contact layers. For the normal and tangential stresses in the contact layer

$$\bar{\sigma}(\bar{x},t) = E_c[\bar{\varepsilon}(\bar{x},t) + \vartheta_c \dot{\bar{\varepsilon}}(\bar{x},t)], \quad \bar{\tau}(\bar{x},t) = G_c[\bar{\gamma}(\bar{x},t) + \eta_c \dot{\bar{\gamma}}(\bar{x},t)] \tag{27}$$

are obtained. The viscous-damping coefficients are related to the loss tangents by

$$\vartheta_c \Omega_{\mathrm{ref}} = \tan\, \delta_{c\vartheta}, \quad \eta_c \Omega_{\mathrm{ref}} = \tan\, \delta_{c\eta} \tag{28}$$

where Ω_{ref} is the circular frequency at which a loss tangent is measured.

The strain $\bar{\varepsilon}$ in the $\bar{z}$-direction and the shear strain $\bar{\gamma}$ in the $\bar{x}-\bar{z}$ direction are approximated by

$$\bar{\varepsilon}(\bar{x},t) = \frac{\bar{w}_c(\bar{x},t)}{h_c}, \quad \bar{\gamma}(\bar{x},t) = \frac{\bar{u}_c(\bar{x},t)}{h_c} \tag{29}$$

Multiplication of Eq. (27) with the width s of the contact model results in

$$\bar{F}_{cN}(\bar{x},t) = k_z \bar{w}_c(\bar{x},t) + d_z \dot{\bar{w}}_c(\bar{x},t), \quad \bar{F}_{cT}(\bar{x},t) = k_x \bar{u}_c(\bar{x},t) + d_x \dot{\bar{u}}_c(\bar{x},t) \tag{30}$$

with

$$k_z = \frac{sE_c}{h_c}, \quad k_x = \frac{sG_c}{h_c}, \quad d_z = \frac{sE_c\vartheta_c}{h_c}, \quad d_x = \frac{sG_c\eta_c}{h_c} \tag{31}$$

In case of isotropic material behavior

$$G_c = \frac{E_c}{2(1+\nu_c)} \tag{32}$$

holds. The virtual work of the inner forces leads to

$$\delta W_{ci} = \int_0^{n_w\lambda} [\bar{F}_{cN}\delta \bar{w}_c + \bar{F}_{cT}\delta \bar{u}_c] d\bar{x} \tag{33}$$

As it was done for the contact forces acting at the stator for the contact layer, the following expression is obtained:

$$\delta W_{cc} = \int_0^{n_w\lambda} -\bar{\mathbf{F}}_c \delta \hat{\bar{\mathbf{u}}}_c d\bar{x} \tag{34}$$

The effect of the tangential contact force, $\bar{F}_T$, on the deformation of the rotor is assumed to be negligible, since $h_r < h_s$ is chosen. Thus, the term $\bar{z}\bar{w}_r'(\bar{x},t)$ in Eq. (3) is ignored when inserted in Eq. (34) resulting in

$$\delta W_{cc} \approx \int_0^{n_w\lambda_s} [\bar{F}_N \delta \bar{w}_c + \bar{F}_T \delta \bar{u}_c + \bar{F}_N \delta \bar{w}_r] d\bar{x} \tag{35}$$

For the contact forces between stator and contact layer, the relation $\mathbf{F}_c(x_P,t) = -\bar{\mathbf{F}}_c(\bar{x}_Q(t),t)$ must hold, where $(x_P, \bar{x}_Q)$ is the coordinates of contacting surface points of stator and rotor, respectively, at time t.

2.4.2 Equations of Motion in Wave Fixed Coordinates. The equations of motion are now derived in a straightforward procedure by carrying out the variations and the partial integrations in Hamilton's principle. Then, a transformation into coordinates of the traveling-wave fixed reference frame is carried out by using Eqs. (7) and (8) and considering Eq. (10). We can then state the stator and rotor equations of motion

$$\rho_s A_s v_w^2 \tilde{w}_s'' + E_s I_s \tilde{w}_s'''' - \eta_s E_s I_s v_w \tilde{w}_s'''''' + k_s \tilde{w}_s = \tilde{M}'' - \tilde{F}_N + \frac{h_s}{2}\tilde{F}_T' \tag{36}$$

$$\rho_r A_r v_w^2 \left(1 - 2\frac{v_r}{v_w} + \left(\frac{v_r}{v_w}\right)^2\right)\tilde{w}_r'' + E_r I_r \tilde{w}_r'''' + k_r \tilde{w}_r = \tilde{F}_N - \tilde{p} \tag{37}$$

2.4.3 Contact Formulation and Contact Laws. Normal and tangential contact forces occur in the contact zone. For normal contact we assume

$$\tilde{F}_N \equiv \begin{cases} \tilde{F}_{cN} & \text{if } \tilde{x} \in [-\tilde{b}, \tilde{c}] \quad : \text{ contact} \\ 0 & \text{if } \tilde{x} \in \left[-\frac{\lambda}{2}, \frac{\lambda}{2}\right] \setminus [-\tilde{b}, \tilde{c}] \quad : \text{ no-contact} \end{cases} \tag{38}$$

whereas for tangential contact the friction law

$$\tilde{F}_T \equiv \begin{cases} \tilde{F}_{cT} & \text{if } \tilde{x} \in [-\tilde{b},\tilde{c}] \wedge \tilde{v}_{\text{rel}} = 0 \quad : \quad \text{stick} \\ \text{sign}(\tilde{v}_{\text{rel}})\mu\tilde{F}_{cN} & \text{if } \tilde{x} \in [-\tilde{b},\tilde{c}] \wedge \tilde{v}_{\text{rel}} \neq 0 \quad : \quad \text{slip} \\ 0 & \text{if } \tilde{x} \in \left[-\frac{\lambda}{2},\frac{\lambda}{2}\right] \setminus [-\tilde{b},\tilde{c}] \quad : \quad \text{no-contact} \end{cases} \tag{39}$$

is used. The forces $\tilde{F}_{cN}$ and $\tilde{F}_{cT}$ in Eqs. (38) and (39) are the material laws, Eq. (30), expressed in coordinates of the traveling-wave fixed reference frame at steady-state

$$\tilde{F}_{cN}(\tilde{x}) = k_z\tilde{w}_c(\tilde{x}) + v_d d_z\tilde{w}_c'(\tilde{x}), \quad \tilde{F}_{cT}(\tilde{x}) = k_x\tilde{u}_c(\tilde{x}) + v_d d_x\tilde{u}_c'(\tilde{x}) \tag{40}$$

We have not distinguished between slipping coefficient μ_{slip} and sticking coefficient μ_{stick}. Wallaschek [1] pointed out that for most of the contacting material pairs in USMs both coefficients are nearly the same.

At the beginning of the contact zone ($\tilde{x}=\tilde{c}$), the contact layer displacement shall satisfy

$$\tilde{u}_c(\tilde{c}) = 0, \quad \tilde{w}_c(\tilde{c}) = 0 \tag{41}$$

In Eq. (41), it is implicitly assumed that the viscous-damping terms d_x and d_z of the contact layer material are sufficiently small, so that the contact layer can expand fast enough to its undeformed configuration before the next wave-crest arrives (see Fig. 4). In case the expansion of the contact layer into its undeformed configuration is not fast enough, two additional unknowns, $\tilde{u}_c(\tilde{c})$ and $\tilde{w}_c(\tilde{c})$, are introduced, which require additional iterations in the solution procedure.

The first boundary condition is obtained at the beginning of the contact zone (point $\tilde{C}$). Taking Eq. (14) at this boundary and considering Eq. (41) yield the following geometrical condition

$$\tilde{w}_s(\tilde{c}) - \tilde{w}_r(\tilde{c}) = 0 \tag{42}$$

which states that contact occurs at point $\tilde{C}$. At the end of the contact zone (point $\tilde{B}$), the normal contact force must vanish due to the beginning of separation. Thus, using Eq. (38) together with Eqs. (40), (14), and (15), gives

$$\tilde{F}_N(-\tilde{b}) \equiv k_z[\tilde{w}_s(-\tilde{b}) - \tilde{w}_r(-\tilde{b})] + v_d d_z\left[-\frac{v_w}{v_d}\tilde{w}_s'(-\tilde{b}) - \tilde{w}_r'(-\tilde{b})\right] = 0 \tag{43}$$

The third condition corresponds to the tangential contact layer displacement at the beginning of the contact zone, see Eq. (41)

$$\tilde{u}_c(\tilde{c}) = 0 \tag{44}$$

2.4.4 Motor Output Force (Torque). At steady-state motor operation, the balance $F_{\text{load}}=F_{\text{motor}}$ holds. The motor output force F_{motor} at steady-state motor operation, shown in Fig. 2, is computed from the tangential contact force $\tilde{F}_T(\tilde{x})$ with

$$F_{\text{motor}} = n_w\int_{-\tilde{b}}^{\tilde{c}} \tilde{F}_T(\tilde{x})d\tilde{x} \tag{45}$$

3 Contact Problem Analysis

In Sec. 2 the equations of motion for the steady-state contact problem of traveling-wave type ultrasonic motors have been derived. The contact problem is given by the contact kinematic equations (14)–(16), the equations of motion of the stator and the rotor in Eqs. (36) and (37), the contact laws for normal and tangential contact in Eqs. (38)–(40), as well as the contact boundary conditions in Eqs. (42)–(44). The given quantities are the axial preload $\tilde{p}$ in Eq. (26), the bending moment excitation $\tilde{M}(\tilde{x})$ in Eq. (22), the traveling-wave speed v_w or the circular excitation frequency Ω, given in Eq. (5), as well as the rotor speed v_r. The displacement functions for stator, rotor and contact layer, $\tilde{w}_s(\tilde{x})$, $\tilde{w}_r(\tilde{x})$, $\tilde{w}_c(\tilde{x})$, and $\tilde{u}_c(\tilde{x})$, the contact boundary coordinates $\tilde{b}$ and $\tilde{c}$, as well as the motor output force F_{motor}, are the unknown quantities.

The solution procedure is divided into four steps. First, in Sec. 3.1, the contact layer displacements are analytically solved and expressed by the stator and rotor displacements. Then, in Sec. 3.2, a Fourier-series expansion of the stator and rotor displacement functions are introduced, and an assumption is stated, which allows one to divide the contact problem into two solution steps: the solution of the normal contact problem and the tangential contact problem. In Sec. 3.3 the normal contact problem is solved independently from the tangential contact problem by first carrying out a Galerkin-discretization and then solving numerically the nonlinear algebraic equations. Owing to the normal contact force distribution taken from the results in Sec. 3.3, only the tangential contact force distribution needs to be calculated. This is done in Sec. 3.4.

3.1 Contact Layer Displacements. The contact layer displacements $\tilde{w}_c(\tilde{x})$ and $\tilde{u}_c(\tilde{x})$ and their derivatives can be expressed by the lateral displacements of stator and rotor within a contact zone $[-\tilde{b},\tilde{c}]$, see Fig. 4. Outside the contact zone, the contact layer displacements are not relevant. By rearranging the normal contact kinematic equations (14) and (15)

$$\tilde{w}_c = \tilde{w}_s - \tilde{w}_r \tag{46}$$

$$\tilde{w}_c' = -\frac{v_w}{v_d}\tilde{w}_s' - \tilde{w}_r' \tag{47}$$

follow.

For calculating the tangential displacement function $\tilde{u}_c(\tilde{x})$, it must be distinguished between a stick or slip-contact state, according to Eq. (39). In a stick-subzone, $\mathcal{U}_i^{\text{stick}} \subset [-\tilde{b},\tilde{c}]$, the tangential displacement of the contact layer results from the condition $\tilde{v}_{\text{rel}}=0$. Solving Eq. (16) for $\tilde{u}_c$ gives

$$\tilde{u}_c^{\text{stick}_i}(\tilde{x}) = -\left(\frac{v_r}{v_d}\tilde{x} + \bar{h}\tilde{w}_r'\right) + \frac{h_s v_w}{2v_d}w_s'(\tilde{x}) + K_i^{\text{stick}} \tag{48}$$

with the integration constant K_i^{stick}. The tangential force for sticking according to Eq. (40) yields

$$\tilde{F}_{cT}^{\text{stick}_i}(\tilde{x}) = k_x\tilde{u}_c^{\text{stick}_i}(\tilde{x}) + v_d d_x\tilde{u}_c^{\text{stick}_i}(\tilde{x})' \tag{49}$$

In a slip-subzone, $\mathcal{U}_i^{\text{slip}} \subset [-\tilde{b},\tilde{c}]$, the tangential contact force follows from Eq. (39) by inserting Eqs. (38) and (40) and substituting $\tilde{w}_c$ with Eqs. (46) and (47)

$$\tilde{F}_T^{\text{slip}_i} \equiv \text{sign}(\tilde{v}_{\text{rel}})\mu[k_z(\tilde{w}_s - \tilde{w}_r) - d_z(v_w\tilde{w}_s' + v_d\tilde{w}_r')] \tag{50}$$

Since $\tilde{F}_{cT}=\tilde{F}_T^{\text{slip}_i}$ holds, the material law in Eq. (40) and the frictional contact force in Eq. (50) can be inserted, resulting in

$$v_d d_x \tilde{u}_c^{\mathrm{slip}_i}(\tilde{x})' + k_x \tilde{u}_c^{\mathrm{slip}_i}(\tilde{x}) = \mathrm{sign}(\tilde{v}_{\mathrm{rel}})\mu[k_z(\tilde{w}_s - \tilde{w}_r) - d_z(v_w \tilde{w}_s' + v_d \tilde{w}_r')] \tag{51}$$

which is a linear inhomogeneous differential equation for the tangential contact layer displacement $\tilde{u}_c^{\mathrm{slip}_i}(\tilde{x})$. The solution is composed of the solution of the homogeneous equation and a particular solution of the inhomogeneous equation

$$\tilde{u}_c^{\mathrm{slip}_i} = \tilde{u}_{ch}^{\mathrm{slip}_i} + \tilde{u}_{cp}^{\mathrm{slip}_i} \tag{52}$$

The solution of the homogeneous equation may be written as

$$\tilde{u}_c^{\mathrm{slip}_i}(\tilde{x}) = \tilde{K}_i^{\mathrm{slip}} e^{-(k_x/v_d d_x)\tilde{x}} \tag{53}$$

and the particular solution

$$\tilde{u}_{cp}^{\mathrm{slip}_i}(\tilde{x}) = \mathrm{sign}(\tilde{v}_{\mathrm{rel}})\tilde{U}_{cp}^{\mathrm{slip}_i}(\tilde{x}) \tag{54}$$

follows under the assumption that $\tilde{w}_s$ and $\tilde{w}_r$ are already known functions from an preceding iteration step. Note that $\tilde{v}_{\mathrm{rel}}$ in Eq. (51) depends on the tangential contact layer displacement $\tilde{u}_c^{\mathrm{slip}}(\tilde{x})$, see Eq. (16). If $\tilde{u}_c^{\mathrm{slip}_i}$ is known, Eq. (52) can be inserted into Eq. (16), yielding

$$\tilde{v}_{\mathrm{rel}} = \frac{h_s}{2} v_w \tilde{w}_s'' - (v_r + v_d \bar{h} \tilde{w}_r'' + v_d[\tilde{u}_{ch}^{\mathrm{slip}_i}(\tilde{x})' + \mathrm{sign}(\tilde{v}_{\mathrm{rel}})\tilde{U}_{cp}^{\mathrm{slip}_i}(\tilde{x})']) \tag{55}$$

The unknown relative velocity occurs on both sides of this equation. However, the resulting value can be found relatively easy by, for example, assuming $\mathrm{sign}(\tilde{v}_{\mathrm{rel}})=1$ in Eq. (55) and computing the resulting $\tilde{v}_{\mathrm{rel}}$. After computation, the sign of $\mathrm{sign}(\tilde{v}_{\mathrm{rel}})$ must be checked if it agrees with the assumption. If not, then $\mathrm{sign}(\tilde{v}_{\mathrm{rel}})=-1$ is valid. The result of $\mathrm{sign}(\tilde{v}_{\mathrm{rel}})$ is then put into Eq. (50).

Depending on the motor's operating conditions, the contact zone $[-\tilde{b},\tilde{c}]$ can be composed of N_c alternating stick and slip subzones, beginning and ending either with a stick-subzone or a slip-subzone

$$[-\tilde{b},\tilde{c}] = \mathcal{U}_1^{\mathrm{slip}} \cup \mathcal{U}_2^{\mathrm{stick}} \cup \mathcal{U}_3^{\mathrm{slip}} \cup \cdots \cup \mathcal{U}_{N_c}^{\mathrm{slip/stick}} \quad \text{or}$$

$$[-\tilde{b},\tilde{c}] = \mathcal{U}_1^{\mathrm{stick}} \cup \mathcal{U}_2^{\mathrm{slip}} \cup \mathcal{U}_3^{\mathrm{stick}} \cup \cdots \cup \mathcal{U}_{N_c}^{\mathrm{slip/stick}} \tag{56}$$

The boundaries of stick and slip-contact subzones are called *transition points* and are denoted by $\tilde{p}_i$, $i=1,\ldots,N_c+1$. It is $\tilde{p}_1=\tilde{c}$ and $\tilde{p}_{N_p}=-\tilde{b}$. It is

$$[-\tilde{b},\tilde{c}] = [\tilde{p}_{N_c+1},\tilde{p}_{N_c}] \cup \cdots \cup [\tilde{p}_2,\tilde{p}_1] \tag{57}$$

The integration constants K_i^{stick} and $\tilde{K}_i^{\mathrm{slip}}$ in Eqs. (48) and (53) must be determined by matching the displacement boundary conditions between stick and slip-contact subzones.

3.2 Fourier-Series Expansion and Contact Problem Formulation. To solve the contact problem, stator and rotor displacements are expressed by Fourier-series expansions

$$\tilde{w}_s(\tilde{x}) = \sum_{n=1}^{N} [A_n \cos(nk\tilde{x}) + B_n \sin(nk\tilde{x})] \tag{58}$$

$$\tilde{w}_r(\tilde{x}) = \tilde{w}_{r0} + \sum_{n=1}^{N} [C_n \cos(nk\tilde{x}) + D_n \sin(nk\tilde{x})] \tag{59}$$

Rigid body deflections, $\tilde{w}_{s0}$ of the stator in the $\tilde{z}$-direction are ignored in Eq. (58). In Sec. 3.1 the contact layer displacements $\tilde{w}_c(\tilde{x})$ and $\tilde{u}_c(\tilde{x})$ have been analytically expressed by the stator and rotor displacements. Thus, no separate Fourier-series expansion of these displacement functions is necessary. Only for the particular solution $\tilde{U}_{cp}^{\mathrm{slip}_i}(\tilde{x})$ in Eq. (54) a Fourier-series expansion is necessary

$$\tilde{U}_{cp}^{\mathrm{slip}_i}(\tilde{x}) = \sum_{n=1}^{N} [E_n^{\mathrm{slip}_i} \cos(nk\tilde{x}) + F_n^{\mathrm{slip}_i} \sin(nk\tilde{x})] + \tilde{K}_{p_i}^{\mathrm{slip}} \tag{60}$$

The unknown parameters are the $4N+1$ Fourier-coefficients $A_1,\ldots,D_N,\tilde{w}_{r0}$, the $(N_c-N_c^{\mathrm{stick}})(2N+1)$ Fourier-coefficients $E_1^{\mathrm{slip}_i},\ldots,F_N^{\mathrm{slip}_i},\tilde{K}_{p_i}^{\mathrm{slip}}$, the N_c integration constants $\tilde{K}_i^{\mathrm{stick}}$ and $\tilde{K}_i^{\mathrm{slip}}$, as well as the two boundary points $-\tilde{b}$, $\tilde{c}$, and the N_c-1 transition points $\tilde{p}_2,\ldots,\tilde{p}_{N_c-1}$. Provided that the coefficient of friction is appreciably less than unity, see Ref. [16], pp. 203–204, the influence of the tangential contact forces on the normal contact forces and on the contact area is small. This allows one to divide the contact problem into the solution of the normal contact problem and the tangential contact problem.

3.3 Normal Contact Problem. The *normal contact problem* is given by the kinematic equations Eqs. (46) and (47), the equations of motion of the stator and the rotor, Eqs. (36) and (37), with $\tilde{F}_T=0$, $v_r=0$, and $F_{\mathrm{motor}}=0$ together with the contact boundary conditions, Eqs. (42) and (43). The given quantities are the axial preload $\tilde{p}$, Eq. (26), the bending moment excitation $\tilde{M}(\tilde{x})$, Eq., (22), as well as the traveling-wave speed v_w or the circular excitation frequency Ω given in Eq. (5). The unknown parameters are the $4N+1$ Fourier-coefficients $A_1,\ldots,D_N$, $\tilde{w}_{r0}$ of the stator and rotor displacement, Eqs. (58) and (59), and the two boundary points $-\tilde{b}$ and $\tilde{c}$.

A global Galerkin-discretization is carried out by inserting Eqs. (22), (26), (58), and (59) into the equations of motion, Eqs. (36) and (37), projecting the resulting equations on the trigonometric functions $\{1,\sin(nk\tilde{x}),\cos(nk\tilde{x})\}$ with $n\in\{1,\ldots,N\}$, and carrying out the partial integrations and integrating over one wavelength, $[-\lambda/2,\lambda/2]$. Here, since $k_z \gg k_r$ holds and both stiffness effects act in parallel, the term $\langle k_r \tilde{w}_{r0},1\rangle$ is set equal to zero. Two additional equations are obtained by inserting Eqs. (58) and (59) into the contact boundary conditions, Eqs. (42) and (43). All together this yields

$$\mathbf{K}(\tilde{b},\tilde{c};\Omega)\mathbf{x} = \mathbf{F} \quad \text{with} \quad \dim \mathbf{K}(\tilde{b},\tilde{c};\Omega) = (4N+3)\times(4N+1) \tag{61}$$

and

$$\mathbf{x} = [A_1,\ldots,A_N,B_1,\ldots,D_N,\tilde{w}_{r0}]^{\mathrm{T}}$$

$$\mathbf{F} = \left[\frac{2\pi}{k}p_0, -4\hat{M}k\sin\left(\frac{\pi}{2}\right),\ldots,-4\hat{M}k\sin\left(N\frac{\pi}{2}\right),0,\ldots,0\right]^{\mathrm{T}} \tag{62}$$

An iterative solution procedure is chosen in order to solve the set of nonlinear algebraic equations, Eq. (61). In an inner loop the Fourier-coefficients and the contact boundaries for a given set of model parameters are computed, and in an outer loop, motor quantities, such as excitation frequency, are varied. In the inner loop, the Fourier-coefficients $\mathbf{x}^{(i-1)}$ in the iteration step $i-1$ follow from a linear equation $\bar{\mathbf{K}}(\tilde{b}^{(i-1)},\tilde{c}^{(i-1)};\Omega)\mathbf{x}^{(i-1)}=\mathbf{F}$ with $\dim \bar{\mathbf{K}}(\tilde{b}^{(i-1)},\tilde{c}^{(i-1)};\Omega)=(4N+1)\times(4N+1)$ at given contact boundaries $\tilde{b}^{(i-1)}$ and $\tilde{c}^{(i-1)}$. By applying Newton's method, for example, the contact boundaries $\tilde{b}^{(i-1)}$ and $\tilde{c}^{(i-1)}$ can be computed in the next iteration step. In the outer loop, a motor parameter is changed incrementally. With this new parameter value, the inner loop is then reactivated. The contact problem is first solved for an elastic contact layer, since $\tilde{c}=\tilde{b}$ and $B_n=0$, $D_n=0$ with $n=1,\ldots,N$ holds due to symmetry reasons. Then the damping parameter d_z is incrementally increased in the outer loop. Before

starting the computation, an estimate of the magnitude of the bending moment excitation $\hat{M}$ in Eq. (62) is required to obtain typical vibration amplitudes in the stator. Therefore, viscous-damping is ignored, $d_z=0$, a vibration amplitude of one micron is chosen ($A_1=1$ μm), and all other Fourier-coefficients are set equal to zero. As an initial guess, the contact boundary is taken to be $\tilde{c}=\lambda/4$. With these assumptions the bending moment excitation $\hat{M}$ can be determined from Eq. (61).

3.4 Tangential Contact Distribution. The stator and rotor displacements, $\tilde{w}_s$ and $\tilde{w}_r$, respectively, the coordinates of the contact boundaries, $(-\tilde{b},\tilde{c})$, and thus the normal contact force distribution $\tilde{F}_N$ are assumed to be known (Sec. 3.3). The tangential displacement $\tilde{u}_c$ and the tangential contact force distribution $\tilde{F}_T$ must be determined for each stick and slip-subzone. The boundaries of neighboring stick and slip subzones are matched by *transition conditions* for the tangential contact force and the tangential displacement.

The *tangential contact problem* is given by the equations for the contact layer displacement functions $\tilde{u}_c^{\text{stick}_i}(\tilde{x})$, Eq. (48) and $\tilde{u}_c^{\text{slip}_i}(\tilde{x})$, Eqs. (51), (53), and (54), together with the kinematic equation, Eq. (55), and the boundary condition Eq. (41). The rotor speed v_r is an input quantity. The output quantities are the displacement function $\tilde{u}_c(\tilde{x})$ and the motor output force F_{motor}. Due to the Galerkin-discretization, the tangential contact problem reduces to the solution of the $(N_c-N_c^{\text{stick}})(2N+1)$ Fourier-coefficients $E_1^{\text{slip}_i},\ldots,F_N^{\text{slip}_i},\tilde{K}_{p_i}^{\text{slip}}$, the N_c integration constants $\tilde{K}_i^{\text{stick}}$ and $\tilde{K}_i^{\text{slip}}$, as well as the N_c-1 transition points $\tilde{p}_2,\ldots,\tilde{p}_{N_c-1}$.

The maximum tangential force distribution for either braking or driving the rotor are stated first

$$\text{braking limit force:}\quad \tilde{F}_T^{l+}(\tilde{x}) := \mu|\tilde{F}_N(\tilde{x})|,$$

$$\text{driving limit force:}\quad \tilde{F}_T^{l-}(\tilde{x}) := -\mu|\tilde{F}_N(\tilde{x})| \tag{63}$$

whereas braking and driving are considered with respect to the rotor rigid body motion v_r. So called *indicator functions* are defined, indicating a transition from either sticking to slipping or vice versa by a change of their sign. The indicator functions may be written as follows.

For stick,

$$\tilde{f}(\tilde{x}) := \mu|\tilde{F}_N(\tilde{x})| - |\tilde{F}_T^{\text{stick}_i}(\tilde{x})|$$

For slip,

$$\tilde{v}_{\text{rel}}(\tilde{x})$$

The sticking contact force $\tilde{F}_T^{\text{stick}_i}$ is obtained by inserting the material law Eq. (40) into Eq. (39)

$$\tilde{F}_{cT}^{\text{stick}_i}(\tilde{x}) = k_x\tilde{u}_c^{\text{stick}_i}(\tilde{x}) + v_d d_x\tilde{u}_c^{\text{stick}_i}(\tilde{x})' \tag{64}$$

where $\tilde{u}_c^{\text{stick}_i}$ is chosen from Eq. (48). The integration constant K_1^{stick} can be obtained from $\tilde{u}_c^{\text{stick}_i}(\tilde{c})=0$ at the beginning of a contact zone, according to Eq. (41). A contact zone starts either with a stick or slip-subzone

$$\tilde{f}(\tilde{c}) > 0 \Rightarrow \text{sticking} \Rightarrow \text{choose}\ \tilde{u}_c^{\text{stick}_1}(\tilde{x}),\quad K_1^{\text{stick}} \tag{65}$$

$$\tilde{f}(\tilde{c}) < 0 \Rightarrow \text{slipping} \Rightarrow \text{calculate}\ \tilde{u}_c^{\text{slip}_1}(\tilde{x}),\quad K_1^{\text{slip}} \tag{66}$$

For the following subzones, a change in the sign of either the force indicator function $\tilde{f}(\tilde{x})$ or the relative velocity indicator function $\tilde{v}_{\text{rel}}(\tilde{x})$ indicates a change of the tangential contact state.

Subzone i is stick-zone,

$$\tilde{f}(\tilde{x}) > 0 \rightarrow \tilde{f}(\tilde{x}) < 0,\quad \tilde{u}_c^{\text{slip}_{i+1}}(\tilde{p}_{i+1}) = \tilde{u}_c^{\text{stick}_i}(\tilde{p}_{i+1}) \Rightarrow K_{i+1}^{\text{slip}}$$

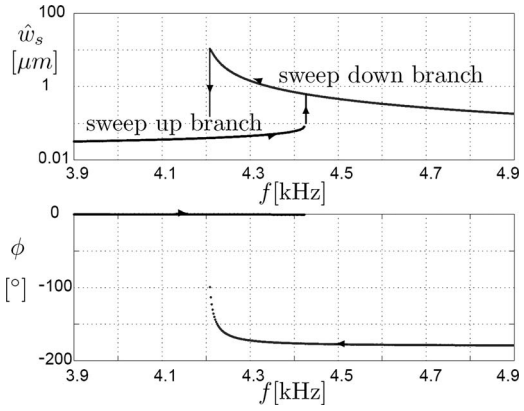

Fig. 5 Nonlinear resonance curve with partial stator-rotor contact ($0<\alpha(\hat{w}_s)<1$)

Subzone i is slip-zone,

$$\tilde{v}_{\text{rel}}(\tilde{x}) > 0 \rightarrow \tilde{v}_{\text{rel}}(\tilde{x}) < 0\quad \tilde{u}_c^{\text{stick}_{i+1}}(\tilde{p}_{i+1}) = \tilde{u}_c^{\text{slip}_i}(\tilde{p}_{i+1}) \Rightarrow K_{i+1}^{\text{stick}}$$

$$\text{slip-zone}\ \ \tilde{v}_{\text{rel}}(\tilde{x}) < 0 \rightarrow \tilde{v}_{\text{rel}}(\tilde{x}) > 0$$

The tangential contact forces from the stick- and slip-contact subzones, Eqs. (64) and (50), are merged, thus, yielding the tangential contact force distribution within the contact zone

$$\tilde{F}_T(\tilde{x}) = \begin{cases} \tilde{F}_T^{\text{stick}_i}(\tilde{x}) & \text{if}\quad \tilde{x}\in\mathcal{U}^{\text{stick}_i} \\ \tilde{F}_T^{\text{slip}_i}(\tilde{x}) & \text{if}\quad \tilde{x}\in\mathcal{U}^{\text{slip}_i} \end{cases} \tag{67}$$

for $i=1,\ldots,N_c$. The motor output force is computed by inserting Eq. (67) into Eq. (45) and carrying out the integration.

4 Results

If not stated otherwise in the figures, the model data are taken from Table 1 in Appendix A. For the subsequent discussion, a nondimensional contact parameter α and a nondimensional normal contact force $\bar{F}_N$ are used, which are both defined in Appendix B, Eqs. (B2) and (B4).

First, the resonance behavior of traveling-wave type ultrasonic motors is considered. In case the stator is not in contact with the rotor, ($\alpha=0$), the resonance frequency of the operational eigenmode is at 42 kHz. If full contact between stator and rotor can be guaranteed, ($\alpha=1$), by applying a sufficiently high axial preload, for example, the resonance frequency shifts to 48 kHz. However, full contact between stator and rotor is counterproductive as driving and braking tangential contact forces would occur simultaneously. In Fig. 5 a typical nonlinear frequency response behavior of the stator vibration amplitude is shown. Starting at an excitation frequency of 49 kHz and following the sweep down branch in Fig. 5 toward lower excitation frequencies, the stator's vibration amplitude increases. Due to this, the contact fraction α decreases according to Fig. 6. In addition, the overall normal contact stiffness between stator and contact layer, $k_{\text{contact}}=k_z A_{\text{contact}}$, decreases, where $A_{\text{contact}}=\alpha(\hat{\tilde{w}}_s)\lambda s$ is the contact area. A decreasing overall contact stiffness makes the stator-rotor contact model more compliant and shifts the resonance to lower values, i.e., toward the limiting resonance frequency $\alpha=0$ at 42 kHz. However, the rate of reduction in the resonance frequency is slower than that of the excitation frequency, so both meet at the frequency of approximately 42 kHz (Fig. 5). Further decrease in the excitation circular frequency causes a jump in the sweep down branch, resulting in a break down of the vibration amplitude. A similar explanation can be given for the sweep up branch. This special nonlinear resonance behavior has also been observed experimentally by Maas et al. [17], for example.

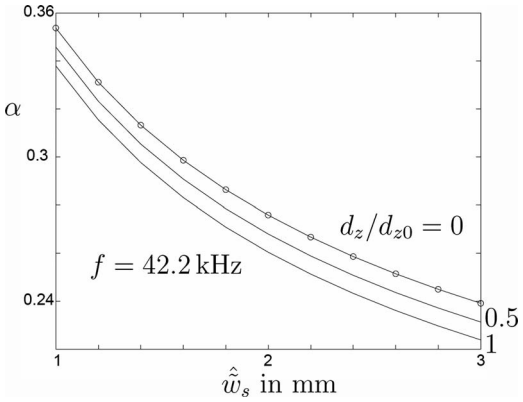

Fig. 6 Contact fraction α versus stator vibration amplitude $\hat{\tilde{w}}_s$ for different viscous-damping coefficients d_z/d_{z0} and d_{z0} from Table 1

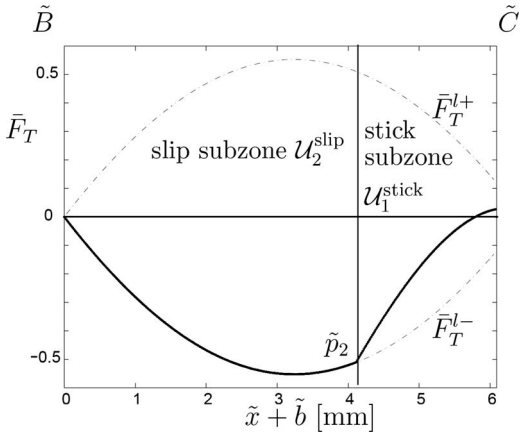

Fig. 8 Typical tangential contact force distribution at $\bar{v}_r=-0.8$, no-load speed: $\bar{v}_r\approx-1$. Thick line: $\bar{F}_T$.

Modeling the rotor as rigid is valid for relatively thick rotors at "moderate" axial pressures p_0. Indeed, to develop efficient motors it is necessary to increase the maximum output torque per volume and to have an eye on "good" transient dynamics of these motors. Therefore, the designer is forced to reduce the rotor weight for fast transient dynamics and to increase the axial pressure in order to increase the motor output torque at constant motor volume. Consequently, the motor design focuses partially on thin and lightweight rotors. Experimental investigations [18] show that under these conditions, rotor flexibility must be taken into account in contact models. The influence of the rotor flexibility on the normal contact behavior and on the speed-force characteristics is illustrated in Fig. 7. It shows the extension of the contact length with decreasing rotor height h_r.

This is accompanied by a smaller compression of the contact layer.

In Figs. 8 and 9, typical distributions of the tangential contact force and the corresponding speeds are illustrated for $\bar{v}_r=-0.8$, i.e., for rotor motion near the no-load speed of $\bar{v}_r\approx-1$, see Appendix B. A stick-subzone U_1^{stick} exists between the beginning of the contact zone at $\tilde{x}=\tilde{c}$ and the transition to slip at $\tilde{p}_2$. In this subzone, the velocity, $\bar{v}_c$, of the contact layer surface points coincides with the velocity, $\bar{v}_s$, of the stator surface points, see Fig. 9. Braking forces ($\tilde{F}_T>0$) exist only in a small region of the stick-subzone. In the second subzone, $\mathcal{U}_2^{\mathrm{slip}}$, from $\tilde{p}_2$ to $\tilde{x}=-\tilde{b}$, slip occurs and it is a driving subzone, since the tangential contact forces are negative.

Figure 10 shows the qualitative change of the tangential contact force distribution with respect to the tangential contact layer stiffness, k_x. The sticking curves become steeper with increasing tangential stiffness and the sticking subzones shrink.

Almost pure slip occurs at $k_x/k_{x0}=100$. In the limiting case, for $k_x/k_{x0}\Rightarrow\infty$, the contact layer displacement in tangential direction results in $\tilde{u}_c=0$. Thus, the tangential velocity of the contact layer simplifies to $v_r\mathbf{e}_x$ (see Eq. (13)). From Eq. (16) it follows, that the relative speed between contact layer and stator surface points can

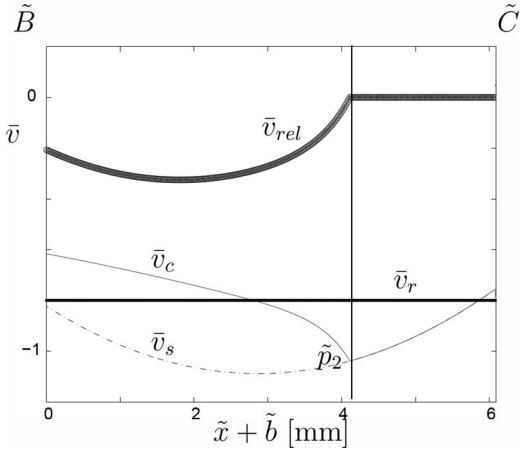

Fig. 9 Typical velocities corresponding to Fig. 8

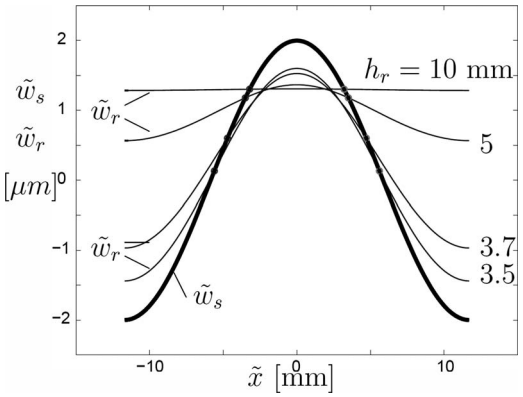

Fig. 7 Rotor deformation at various rotor heights; ○ contact boundaries

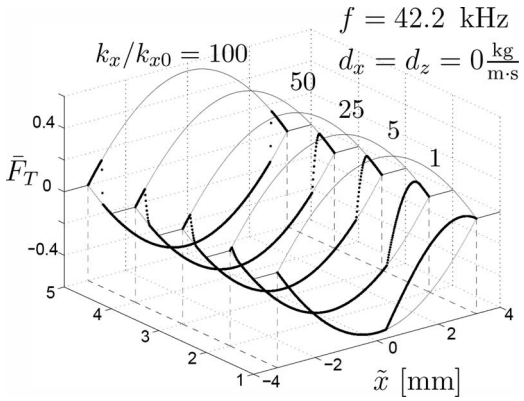

Fig. 10 Tangential contact force distribution for the variation in the tangential contact layer stiffness k_x; k_{x0} from Table 1

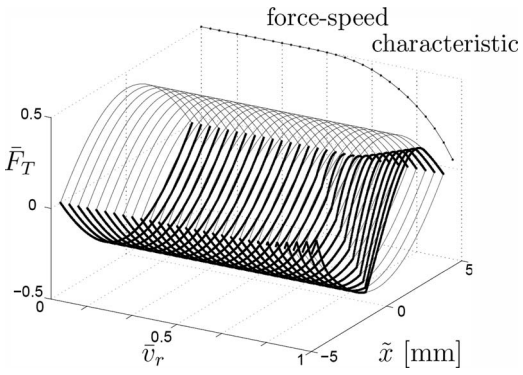

Fig. 11 Tangential contact force distribution for a particular speed-force characteristic

only be zero at singular points $\tilde{x}^*$ for which $h_s/2v_w\tilde{w}_s''(\tilde{x}^*)=v_r$ is valid. Hence, except for singular points in the contact zone, only slip exists between the stator and contact layer. Such a behavior is obtained when neglecting the tangential displacement of the contact layer. A drastic overestimation of the wear losses may result. Figure 11 illustrates the tangential contact force distribution along a particular speed-force characteristic. Near the no-load speed, the driving ($\bar{F}_T<0$) and braking tangential contact forces ($\bar{F}_T>0$) nearly cancel each other and complicated contact states occur containing several stick-slip subzones.

Figure 12 shows the influence of the stator vibration amplitude on the speed-force curves. The no-load speed increases proportionally to the increase in the stator vibration amplitude. The stall-force (force at $\bar{v}_r=0$) stays unchanged. In Fig. 13 the influence of the axial pressure $\bar{p}$ on the speed-force characteristics is shown. Naturally, the stall-force increases linearly with increasing axial pressure. However, the no-load speed decreases due to the increase of the contact length. Additionally, the speed drop is less distinct with increasing loading force.

As would be expected, a variation of the contact layer height influences the normal contact layer stiffness, as well as the tangential contact layer stiffness in Eq. (40). Since the contact length increases with increasing contact layer height, the no-load speed decreases, see Fig. 14. A more compliant rotor may lead to a more distinct speed drop along with increasing motor force $\bar{F}_{\text{motor}}$. This is illustrated in Fig. 15, where the corresponding speed-force characteristics for different rotor heights are shown.

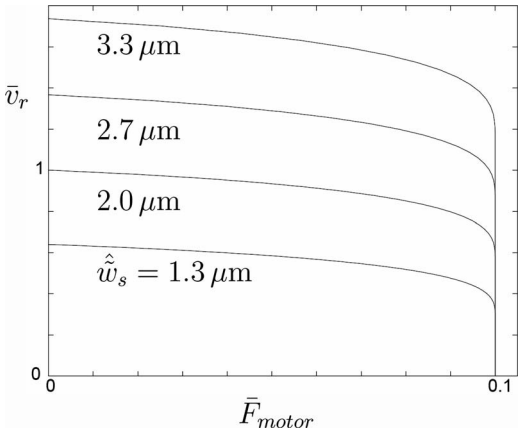

Fig. 12 Speed-force characteristics for various stator vibration amplitudes, $\hat{\tilde{w}}_s$

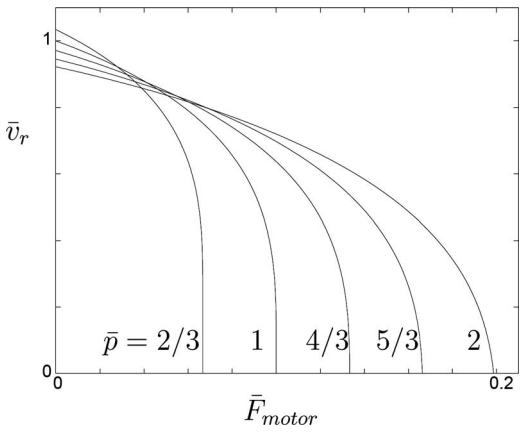

Fig. 13 Speed-force characteristics for various axial pressures $\bar{p}$

5 Conclusions

The contact problem between rotor and stator of ultrasonic traveling-wave motors leads to a nonlinear resonance with distinct jump phenomena. Near the resonance peak, the feedback of the rotor dynamics on the stator vibration is negligible, resulting in an almost harmonic stator vibration. Depending on the motor force $\bar{F}_{\text{motor}}$ and the rotor speed $\bar{v}_r$, a complicated contact state with several stick and slip subzones within one contact zone may occur. Information about stick and slip subzones is useful in studying the efficiency and the wear properties of contact layer mate-

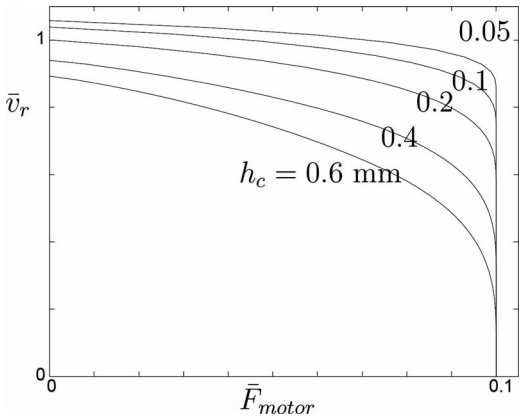

Fig. 14 Speed-force characteristics for various contact layer heights

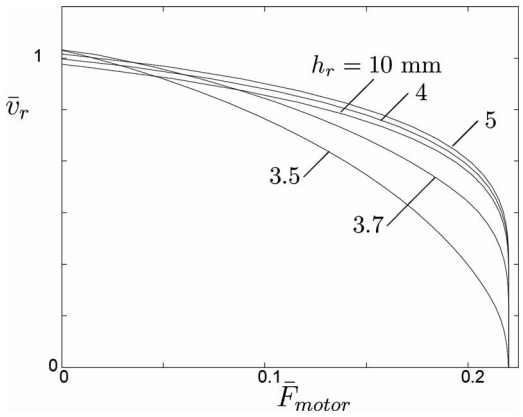

Fig. 15 Speed-force characteristics for various rotor heights

Table 1 Data of the reference model for the numerical analysis

Symbol	Reference value	Dimension
λ	2.34×10^{-2}	m
n_w	11	
s	5.6×10^{-3}	m
h_s	6.54×10^{-3}	m
h_r	3.5×10^{-3}	m
h_c	2×10^{-4}	m
ϱ_s	8.8×10^{3}	kg/m^3
ϱ_r	2.65×10^{3}	kg/m^3
E_s [a]	$0.3\times1.1\times10^{11}$	N/m^2
E_r	7×10^{10}	N/m^2
E_c	1×10^{9}	N/m^2
ν_c	0.3	
F_{axial}	900	N
$k_s,\ k_r$	5×10^{7}	N/m^2
$\tan\delta_c$ [b]	0.1	
η_s	0	s
Ω_{ref}	$2\pi\times42,200$	rad/s
μ	0.1	

[a]Young's modulus is multiplied by 0.3 to adjust the eigenfrequency of the stator model to that of a physical stator.
[b]Used for both normal and tangential direction, see Ref. [14], p. 292.

rials. The characteristic that the speed drops as the motor force increases can be strongly influenced by changes in the stiffness of the contact layer, as well as of the rotor. With relatively stiff contact layer material and rotor, the rotor speed is nearly constant over a wide range of motor forces. Desired speed-torque characteristics may be obtained through proper design of the motor without additional control effort. Despite this, a good understanding of the motor behavior would be useful when designing a controller for USMs.

To summarize, it can be said that the mathematical model presented and analyzed in this paper can be used as a tool for optimizing the design of ultrasonic traveling-wave motors in steady-state operation.

Appendix A: Table of Reference Data

The reference data are shown in Table 1.

Appendix B: Nondimensional Model Quantities

For the presentation of the results it is useful to scale the contact model quantities. Therefore, three characteristic quantities are introduced a characteristic axial preload, $[F_{\text{axial}}]$, a characteristic normal pressure, $[p]$, and a characteristic no-load speed, $[v_r]$

$$[F_{\text{axial}}] := F_{\text{axial}}, \quad [p] := \frac{F_{\text{axial}}}{n_w\lambda}, \quad [v_r] := \frac{h_s\Omega_{\text{ref}}}{2\tilde{c}^*}\tilde{w}_s(\tilde{c}^*) \tag{B1}$$

The model data are taken from Table 1. The nondimensional field quantities of the contact forces are

$$\bar{F}_N(\tilde{x}) := \frac{\tilde{F}_N(\tilde{x})}{[p]}, \quad \bar{F}_T(\tilde{x}) := \frac{\tilde{F}_T(\tilde{x})}{[p]} \tag{B2}$$

and the nondimensional motor parameters will be given as

$$\bar{F}_{\text{axial}} := \frac{F_{\text{axial}}}{[F_{\text{axial}}]}, \quad \bar{F}_{\text{motor}} := \frac{F_{\text{motor}}}{[F_{\text{axial}}]}, \quad \bar{v}_x := \frac{v_x}{[v_r]}, \quad x \in s,r,c \tag{B3}$$

Additionally, a nondimensional contact length is introduced according to

$$\alpha := \frac{\tilde{c}+\tilde{b}}{\lambda}, \quad \alpha \in [0,1] \tag{B4}$$

The characteristic normal pressure, see Eq. (26), describes the contact pressure between stator and rotor for the stator at rest. The characteristic no-load speed, $[v_r]$, is defined as the speed of the rotor at $F_{\text{motor}}=0$ in Eq. (45) for a particular *reference no-load motor operation state*. In this case, the driving and braking forces of $\tilde{F}_T(\tilde{x})$ in Eq. (67) must cancel each other. Equation (B1) is obtained by assuming a pure stick condition, i.e., $\tilde{v}_{\text{rel}}=0$, as well as ignoring damping effects ($d_x=d_z=0$) and subsequently inserting Eqs. (39), (40), and (48) into Eq. (45) and carrying out the integration procedure. The integration constant K^{stick} in Eq. (48) is determined by taking the boundary condition in Eq. (44) into account. The reference no-load motor operation state requires the determination of the reference normal contact state. Therefore, the variables $\tilde{c}^*$ and $\tilde{w}_s(\tilde{c}^*)$ must be computed for a contact model with rigid rotor $\tilde{w}_r'(\tilde{x})=0$ and $d_x=d_z=0$. The bending moment excitation $\hat{M}$ is adjusted to give a stator vibration amplitude of $\hat{\tilde{w}}_s^*=2\ \mu$m. The reference normal contact state then yields $\tilde{c}^*=3.25$ mm, $\tilde{w}_s(\tilde{c}^*)=1.75\ \mu$m, and thus $[v_r]=0.47$ m/s follows.

The motor output force at zero rotational speed is called the stall-force. Assuming a pure slip tangential contact state at stall-force, this force may be computed by the equation $F_{\text{motor}}^*=\mu F_{\text{axial}}$. Dividing this equation by $[F_{\text{axial}}]$ and taking the friction coefficient from Table 1 results in $\bar{F}_{\text{motor}}^*=0.1$. Now, a *reference no-load speed* and a *reference stall-torque* are defined at $\bar{F}_{\text{axial}}=1$: $\bar{v}_r^* := 1$, $\bar{F}_{\text{motor}}^* := 0.1$. In the case of a rotational USM with diameter 90 mm, for example, these data yield no-load speed: $U^*=100$ rpm, stall-torque: $T^*=4$ Nm.

References

[1] Wallaschek, J., 1998, "Contact Mechanics of Piezoelectric Ultrasonic Motors," Smart Mater. Struct., **7**, pp. 369–381.
[2] Zharii, O., and Ulitko, A. F., 1995, "Smooth Contact Between the Running Rayleigh Wave and a Rigid Strip," ASME J. Appl. Mech., **62**, pp. 362–367.
[3] Le Moal, P., and Minotti, P., 1997, "A 2-D Analytical Approach of the Rotor/Stator Contact Problem Including Rotor Bending Effects for High Torque Piezomotor Design," Eur. J. Mech. A/Solids, **16**(6), pp. 1067–1103.
[4] Cao, X., and Wallaschek, J., 1995, "Estimation of the Tangential Stresses in the Stator/Rotor Contact of Travelling Wave Ultrasonic Motors Using Visco-Elastic Foundation Models," *Second International Conference on Contact Mechanics, Contact Mechanics II*, Ferrara, Italy, Computational Mechanics, Southhampton, Boston, MA, pp. 53–61.
[5] Schmidt, J., Hagedorn, P., and Bingqi, M., 1996, "A Note on the Contact Problem in an Ultrasonic Travelling Wave Motor," Int. J. Non-Linear Mech., **31**(6), pp. 915–924.
[6] Hagood, N. W., IV, and McFarland, A. J., 1995, "Modeling of a Piezoelectric Rotary Ultrasonic Motor," IEEE Trans. Ultrason. Ferroelectr. Freq. Control, **42**(2), pp. 210–224.
[7] Hagedorn, P., Sattel, T., Speziari, D., Schmidt, J., and Diana, G., 1998, "The Importance of Rotor Flexibility in Ultrasonic Traveling Wave Motors," Smart Mater. Struct., **7**, pp. 352–368.
[8] Hagedorn, P., and Wallaschek, J., 1992, "Travelling Wave Ultrasonic Motors, Part I: Working Principle and Mathematical Modelling of the Stator," J. Sound Vib., **155**(1), pp. 31–46.
[9] Sashida, T., and Kenjo, T., 1993, *An Introduction to Ultrasonic Motors*, Clarendon, Oxford.
[10] Wriggers, P., 1995, "Finite Element Algorithms for Contact Problems," Arch. Comput. Methods Eng., **2**(4), pp. 1–49.
[11] Maeno, T., Takayuki, T., and Miyaki, A., 1992, "Finite-Element Analysis of the Rotor/Stator Contact in A Ring-Type Ultrasonic Motor," IEEE Trans. Ultrason. Ferroelectr. Freq. Control, **39**(6), pp. 668–674.
[12] Honda, T., and Kato, K., 1993, "Fundamental Properties of Friction and Wear on Friction Drive by Traveling Wave Type Ultrasonic Motors," Jpn. J. Tribol., **47**(7), pp. 1073–1084.
[13] Flynn, A., 1997, "Piezoelectric Ultrasonic Micromotors," Ph.D. thesis, MIT Artificial Intelligence Laboratory, Cambridge, MA.
[14] Ueha, S., Tomikawa, Y., Kurosawa, M., and Nakamura, N., 1993, *Ultrasonic*

Motors Theory and Applications, Clarendon, Oxford.
[15] Rehbein, P., and Wallaschek, J., 1998, "Friction and Wear Behaviour of Polymer/Steel and Alumina/Alumina Under High-Frequency Fretting Conditions," Wear, **216**, pp. 97–105.
[16] Johnson, K. L., 1985, *Contact Mechanics*, Cambridge University Press, Cambridge, England.
[17] Maas, J., Schulte, Th., Grotstollen, H., and Froehleke, N., 1999, "Model-Based Control of Traveling Wave Type Ultrasonic Motors," *Proceedings of the Third International Heinz Nixdorf Symposium*, Heinz Nixdorf Institut, Paderborn, Germany.
[18] Sattel, T., and Hagedorn, P., 2000, "On the Contact Between Rotor and Stator in an Ultrasonic Traveling Wave Motor," *Proceedings of the Eighth International Symposium on Transport Phenomena and Dynamics of Rotating Machinery*, Vol. II, Paper No. ISROMAC-8.